

Derivation of sky view factors from LIDAR data

Chris Kidd^{*†} and Lee Chapman[‡]

[†]Earth System Science Interdisciplinary Center, University of Maryland, and
NASA/Goddard Space Flight Center, Greenbelt, Maryland, 20771, USA.

[‡]School of Geography, Earth and Environmental Sciences, The University of
Birmingham, Edgbaston, Birmingham. B15 2TT. UK.

Abstract

The use of Lidar (Light Detection and Ranging), an active light-emitting instrument, is becoming increasingly common for a range of potential applications. Its ability to provide fine resolution spatial and vertical resolution elevation data makes it ideal for a wide range of studies. This paper demonstrates the capability of Lidar data to measure sky view factors (SVF). The Lidar data is used to generate a spatial map of SVFs which are then compared against photographically-derived SVF at selected point locations. At each location three near-surface elevations measurements were taken and compared with collocated Lidar-derived estimated. It was found that there was generally good agreement between the two methodologies, although with decreasing SVF the Lidar-derived technique tended to over-estimate the SVF: this can be attributed in part to the spatial resolution of the Lidar sampling. Nevertheless, airborne Lidar systems can map sky view factors over a large area easily, improving the utility of such data in atmospheric and meteorological models.

1. Introduction

Geospatial information has become increasingly important to government and commercial agencies for a range of applications. This includes the collection, processing and application of space-height data derived from airborne Lidar sensors. Lidar (also know as airborne laser scanning; ALS) provides high density, high-resolution, accurate 3D point data acquisition and makes directly the availability of 3D points in object space (Habib et al, 2005). Airborne lidar in particular provides one of the most effective and reliable means of terrain data collection. A full review of Digital Elevation Model (DEM) generation techniques from LIDAR can be found in Liu (2008).

The generation of DEMs is not new: digital data bases have been digitised from map data, which in turn had been generated through ground surveys. However, the level of detail on these DEMs was typically low, and could only be used to provide crude sky-view information. In addition, such DEMs were generated to represent the earth surface, rather than the actual surface. More recently large-area DEMs have included those derived from Shuttle Radar Topography Mission (SRTM; Berry et al. 2007) with a best resolution of 1 arc-second (~30 m) or the Advanced Spaceborne Thermal Emission and Reflectance Spectrometer (ASTER) as described by Hirano (2003). Fisher and Tate (2006) provide an overview and discussion of the errors associated with DEM generation.

Lidar-generated DEMs in particular, have undergone significant development in the last 10-15 years. Interest in its ability to capture higher levels of detail than satellite-

derived instrumentation has grown as the level of detail in associated imagery has increased. In particular, using Lidar to obtain elevation data has a number of advantages including the ability to survey large areas quickly with a high-level of detail. It can provide a comprehensive survey, even in areas of limited or restricted access, while the resulting terrain model can be easily combined with other geospatial information. Lidar therefore provides a cost-effective means for the collection and exploitation of accurate height information.

Although Lidar is very adept at obtaining data for DEM generation it is unable to penetrate water, and often cannot retrieve over water due to the specular reflection of the laser beam off the water surface. In addition, it has difficulty in retrieving unambiguous ground levels under dense vegetation canopies, although winter-time provides better coverage due to thinner tree canopies. However, a number of studies have shown that Lidar has the ability to retrieve vegetation height: through the analysis of the first and last return of the laser pulse the height of vegetation and trees vs the surface may be obtained (see Kraus and Pfeifer, 1998). Indeed, Devereux et al. (2005) and Suarez et al. (2005) showed that archeological features could still be identified under woodland.

The drive for greater spatial resolution has greatly enhanced/improved the potential for site-specific exploitation of these data. Consequently, Lidar has become an invaluable tool in the observation of the Earth and, through combination with other data sets, the exploitation of Earth observation data sets in general. It has found uses in landscape mapping, identifying archeological features (e.g. Bewley et al. 2005; Devereux et al. 2008), while Howard et al. (2008) studied archeological remains on the flood plain of the Trent Valley. Applications in the physical environment have included river environments. Charlton et al. (2003) investigated the cross-profiles of gravel-beds in rivers, comparing the Lidar surface with a surface survey. They found that vegetation and water depth affected the accuracy of the Lidar data, although for unvegetated exposed bars, it was capable of providing high-resolution information.

The ability of Lidar to obtain high-resolution 3D data creates the potential to calculate sky-view factors (SVF) from the derived DEM. The SVF is a measure of the amount of sky visible at a particular location: it is a dimensionless parameter, ranging from 0 (obscured view) to 1 (unobscured view). SVFs were identified by Chapman and Thornes (2006) as a key geographical parameter affecting surface radiation budgets, and therefore critical in the accurate monitoring and forecasting of surface temperatures. Their results show that SVF plays a dominant role in the prediction of road surface temperatures. However, despite its importance, the calculation of SVFs is challenging. Conventional measurements have relied upon geometry: simple trigonometry from site surveys establish building/object heights and subsequently lines of sight (e.g. Oke 1981). However, surveying techniques are somewhat limited and time consuming, and often rely upon a number of samples to calculate the full SVF. Use of photographic techniques with fish-eye lenses have greatly aided the collection of the initial data, allowing a full hemisphere to be viewed at once. Subsequent processing of the data is possible through manual analysis (e.g. Steyn, 1980) or through automated image processing techniques (e.g. Blennow, 1995; Grimmond et al. 2001; Chapman et al. 2001). Although "automated", such techniques require supervision and the separation of scene from sky is not always clearly delineated. In particular, the quality of the photographic recording of the photography is critical in the final analysis: consistent light levels are ideal, due to problems such as variations in light level (due to cloud),

pixel saturation (due to direct sun) etc. Some of these issues can be partially resolved by using non-visible imagery (e.g. Postgard & Nunez, 2002; Chapman et al. 2007). Many applications require the batch processing of imagery for thousands of sites and thus, semi-automated techniques which still require user-intervention are not ideal.

Another technique that has attracted some attention for the derivation of SVF is the use of Global Positioning System (GPS) satellite visibility. This method relies upon the premise that the number of satellites “visible” to the GPS receiver at any location is related to the amount of open sky. In a pilot study (Chapman et al. 2002) using 112 sites it was found that 88% of variance in the SVF in urban areas could be explained by the GPS signals. A further study by Chapman and Thornes (2004) used an artificial neural network (ANN) to model the SVF based upon GPS signals. They noted that issues arose relating to lag/lead times for the GPS receiver to attain (and discard) signals, possibly due to the blocking effects of the buildings or vegetation. In urban areas the GPS-ANN technique explained 69% of the variance or photographically-derived SVF, but in rural areas this fell to 45%. This could be explained primarily due to greater image complexity with a greater fraction of vegetation cover (and variation), leading to greater segmentation of the SVF compared with the hard-engineering of urban areas. Thus land-use cover is itself a controlling factor in the accuracy of SVF retrievals.

In the quest for continuous and automated measurements of SVF, the most recent approaches have largely been developed in a GIS environment. Although this ray tracing approach is not new (e.g. Souza et al. 2003; Teller & Azar, 2001), this now appears to be the preferred choice for calculating SVF for large areas (e.g. Unger, 2009). Studies have utilised a variety of vector and raster datasets for calculation (e.g. Gal et al. 2009), however the accuracy of the input data is crucial. To date no SVF study has directly utilised Lidar as a potential source of high resolution 3D raster data, therefore this paper investigates the usefulness of Lidar-derived DEMs in the generation of SVFs compared with existing photographic techniques. The potential of the Lidar system is to generate a spatial map of SVF which can be compared with point-location SVF as derived from current techniques: this ability to capture the spatial variability of SVF has significant advantages when used in the calculation of local and regional-scale energy budgets.

2. Methodology

A study area in southeast Cornwall (UK) was selected for the comparison between the photographic SVF retrieval and the Lidar SVF retrieval (figure 1). This region contains a diverse range of land uses including sea, urban, rural and woodland, providing a good range of SVF values. Lidar data was obtained from the UK Environment Agency covering an area of 2 x 2 km. The data has a nominal horizontal resolution of 2 m: heights were provided in mm, although the absolute accuracy is typically in the region of 60-160 mm. Figure 2 shows the area covered by the Lidar data: light areas indicate higher regions, which dark areas represent lower regions. In addition to the general topographical features, man-made features can be observed, such as hedgerows, buildings and roads. A suitable transect was selected and measurements taken at 30 locations that were representative of land uses in this area. The positions of the sample sites were found by GPS to enable co-registration of the surface and Lidar data sets.

Surface SVF were generated from digital photographs taken with a Nikon N950 and Nikon fish-eye lens attachment. At each location, photographic imagery was taken at heights of 0, 1 and 2 m above the ground using a specially devised plate for the

surface measurement and a tripod for the 1 and 2 m measurements. The images were taken at dusk with no cloud cover, thus minimising problems associated with variations in the light levels, leading to improved classification of the 'sky' in the resulting images (Chapman et al. 2001). Despite the abundance of techniques to calculate SVF from fisheye imagery in the literature, no standard technique exists. For this reason, the opportunity was taken to try a new approach which would yield comparable results whilst providing additional information pertaining to error in the delineation process. Images were processed using the Erdas/Imagine software to generate an unsupervised classification: this was chosen due to its speed and simplicity. Each image produced 3-4 classes that could be associated with clear sky, about 9-10 classes that were associated with the surface and 2-3 classes that were deemed indeterminate. Additional post processing was undertaken to remove any spurious 'sky' in the non-sky region and vice versa. The remaining unassigned regions may be thought of as uncertainties in the photographic SVF classification scheme. An example of the imagery and subsequent processing can be seen in figure 3: the initial image (figure 3(a)) shows the fish-eye photograph orientated with the centre being vertically upwards. It can be noted there is some variation in the lightness of the sky caused by atmospheric scattering. Processing of this image through an unsupervised classification scheme produces figure 3(b), where the grey-shades represent each of the different classes. The final image (figure 3(c)) is generated by combining the sky classes and non-sky classes together, while leaving the indeterminate classes as a measure of uncertainty. A program was then used to calculate the fractional coverage of the sky, indeterminate and non-sky pixels in each image. This methodology was applied to all 30 locations at each of the three heights: an example of the photographically-derived SVF with height can be seen in figure 4.

The Lidar-derived SVF map was calculated using a bespoke program: for each 2 m Lidar sample all the surrounding points are scanned and the elevation angle between the current location and the distant point is calculated. The level of detail required was based upon a number of trials, consequently the SVF factor was based upon scan (azimuth) angles ranged from 0 to <360 degrees in increments of 0.1 degrees, with points up to 1000 m distant (or edge of data region) being considered in the calculations (see figure 5). The choice of the maximum distance is a critical factor and needs changing when considering the larger-scale surface morphology, but was deemed appropriate for the present study. The greatest elevation angle per azimuth angle was recorded and used to calculate the SVF as a fraction of the maximum possible SVF defined for a clear hemisphere of the sky. To match the surface samples at 0, 1 and 2 m, the Lidar-derived SVF was also generated at these heights. The resulting Lidar-derived SVF map can be seen in figure 6: the light areas indicate regions of relatively open sky (SVF~1) while the darker regions indicate lower SVF values. Man-made features dominate much of the textural information with the urban areas and hedgerows being apparent, together with woodland. Similar maps were generated for the surface +1 m and the surface +2 m. Of particular note is that the Lidar-derived surface SVF map revealed some fine-scale noise: this appeared to be associated with the scanning. This had the effect of increasing the relative pixel-pixel noise, and thus affecting the calculated SVF at each pixel. However, this effect was drastically reduced, if not eliminated using the +1 and +2 m SVF maps.

Once the Lidar SVF map had been generated, it was interrogated to retrieve the Lidar-derived SVF for comparison with the photographic technique. The

latitude/longitudes from the GPS unit were converted to the British National Grid and to the x/y of the lidar image, whereby the SVF for the matched pixel was retrieved. In addition to the calculated Lidar SVF, the minimum and maximum SVF of the adjacent pixels were also retrieved to help determine the variability of SVF in the locality and account for possible geo-registration problems.

3. Results

An initial pilot study was carried out to test the ability of the Lidar data to produce realistic SVF data. This study compared a number of photographic SVF images with those generated through remapping the Lidar data to a fish-eye projection, allowing direct visual comparison between the two images. Examples of this comparison are shown in figure 7. The first example, figure 7(a), shows an enclosed area with two tall tower blocks being visible in both the photographic and Lidar images, although there is slight mis-registration probably due to imprecise ground locations (i.e. GPS error). The second example, figure 7(b), is of a more open situation. The relative location of the buildings along the horizon in both the photographic and Lidar images is well represented, and even individual trees can be discerned. It is also clear from figure 6 that the Lidar generates a visually realistic and comprehensible SVF map: the lowest SVF values are within the urban areas and in areas of woodland where the sky view is limited by the proximity to buildings and tree canopies. The highest SVF values are in the more open regions, particularly at the top of the local relief.

To help ascertain the ability to Lidar to quantitatively derive SVF two approaches were used. The first compares the Lidar-derived and the photographically-derived SVF along the transect of the route shown in figure 1. This SVF transect is shown in figure 8 and includes the surface, +1 and +2 m SVF for both methodologies: the continuous lines in figure 8 are the Lidar-derived SVFs, while the photographic SVF are represented by the dots. It can be seen that the SVF varies substantially along the transect, with the sections through the village having the lowest and most variable SVFs, while the more rural areas show higher SVF: this is true for both techniques. Taking the Lidar-derived SVFs, the surface values have some significant pixel-to-pixel variations, particularly along the open lane section. As noted in the methodology section, there was some noticeable noise in the Lidar data, consequently when calculating the SVF the noise within the values of the adjacent pixels propagated through to the SVF value for that pixel. By 'increasing' the height of the location by 1 (or 2) m raises it above this local noise and provides a much smoother transect than at the surface. A similar effect might be expected with the photographically-derived SVF, where the 'noise' is the 'clutter' close the point of observation, such as benches, signs, low vegetation etc. However, it is not clear from figure 8 whether this is significant due to the single point-retrievals of SVF using this method. Nevertheless, there is some degree of agreement between the two methodologies shown in figure 8.

Further comparisons of the methodologies were performed through the plotting of the point-location SVF: these are shown the scatterplots in figure 9(a-c). These plots show generally good agreements between the photographic SVF and the lidar-derived SVF, although with obvious deviations where more obscured sky conditions exist: R^2 values of 0.71, 0.77 and 0.77 were obtained for the 0, 1 and 2 m levels respectively. These results are comparable, and indeed better, than GPS techniques which have become a standard technique in continuous SVF measurement (e.g. Chapman & Thrones, 2004). The increase between the 0 and 1m level can be attributed in part to the

removal of noise effects in the Lidar data. The improvement in the R^2 value with increasing height may be attributed in part to two factors. First, the calculation of the SVF in areas where there is overhanging vegetation (i.e. woodland or close to hedgerows) can be difficult for both photographic and lidar techniques. In particular, there is no guarantee that the Lidar 'surface' that is being used is the actual ground surface. Consequently in some wooded areas the Lidar 'surface' could relate to the canopy, thus generating a higher SVF than would be measured at the ground. Second, within urban areas with narrow street 'canyons' the horizontal sampling of the Lidar is critical. In this study a sampling resolution of 2 m was available which was probably too coarse to ensure that all the narrow streets are properly resolved in the final product.

Despite inadequacies in the generation of SVF from photographic imagery the level of uncertainty is relatively small. It was found that using the unsupervised classification scheme and post-processing the highest degree of uncertainty was about ± 0.05 : this tended to be for the locations where overhanging vegetation was greatest. Calculation of uncertainties in the Lidar SVF values is less direct. However, errors can be attributed to a number of sources including the (relative) accuracy of Lidar height measurements and the location of the sample point on the DEM, particularly in regions where there are large spatial variations in SVF.

4. Conclusion

This study has demonstrated the use of Lidar-derived DEMs to derive values of SVF spatially. Comparison with photographically-derived SVF indicates that there is reasonable agreement, except in areas where vegetation is dominant. In addition, errors from the geo-registration of the sample points vis-à-vis the Lidar data and the horizontal resolution can be significant. The increase in the horizontal resolution of the DEM to <1 m would significantly increase the practical utility of the data. This, in particular, is critical for use in the urban environment where due to the greater variety of land uses the scale-length, or surface roughness, is much greater than that found in the open countryside.

There is therefore a trade off between the better-quality point photographic method and the Lidar-derived method with spatial coverage and vastly reduced fieldwork costs. With improving horizontal resolutions, up to 0.25 m now available, the ability of the Lidar to identify and measure the surface features accurately and hence derive more accurate SVF will be possible.

Acknowledgements

We would like to thank the UK Environment Agency for provision of the Lidar data set. We would also like to thank the reviewers for their thoughts and recommendations.

References.

- BERRY, P.A.M., GARLICK, J.D. and SMITH, R.G., 2007, Near-global validation of the SRTM DEM using satellite radar altimetry. *Remote Sensing of Environment* **106**, pp17-27
- BLENNOW, K., 1995, Sky view factors from high-resolution scanned fish-eye lens photographic negatives. *Journal of Atmospheric and Oceanic Technology* **12**, pp1357-1362.

- BURGESS, T., 2004: Investigation of Fli-map system for Flood Defence asset monitoring. R&D technical report W5A-059/1/TR. Environment Agency, Bristol. ISBN 1857058852
- CHAPMAN, L., THORNES, J.E. and BRADLEY, A.V., 2001, Rapid determination of canyon geometry parameters for use in surface radiation budgets. *Theoretical and Applied Climatology* **69**, pp81-89
- CHAPMAN, L., THORNES, J.E. and BRADLEY, A.V., 2002, Sky-view factor approximation using GPS receivers. *International Journal of Climatology* **22**, pp615-621.
- CHAPMAN, L. and THORNES, J.E., 2004, Real time sky-view factor calculation and approximation. *Journal of Atmospheric and Oceanic Technology* **21**, pp730-741
- CHAPMAN, L. and THORNES, J.E., 2006, A geomatics-based road surface temperature prediction model. *Science of the Total Environment* **360**, pp68-80. doi: 10.1016/j.scitotenv.2005.08.025
- CHAPMAN, L., THORNES, J.E., MULLER, J.P. & MCMULDROCH, S., 2007, Potential applications of thermal fisheye imagery in urban environments *Geoscience and Remote Sensing Letters* **4**, pp56-59
- FISHER, P.F. and TATE, N.J., 2006, Causes and consequences of error in digital elevation models. *Progress in Physical Geography* **30**, pp467-489. doi: 10.1191/0309133306pp492ra
- GAL, T., LINDBERG, F. and UNGER, J., 2009, Computing continuous sky view factors using 3D urban raster and vector databases: comparison and application to urban climate. *Theoretical and Applied Climatology* **95**, pp111-123
- GRIMMOND, C.S.B., POTTER, S.K., ZUTTER, H.N. and SOUCH, C., 2001, Rapid methods to estimate sky-view factors applied to urban areas. *International Journal of Climatology* **21**, pp903-913. doi: 10.1002/joc.659
- HABIB, A., GHANMA, M., MORGAN, M. and AL-RUZOUQ, R., 2005, Photogrammetric and LiDAR data registration using linear features. *Photogrammetric Engineering and Remote Sensing* **71**, pp699-707.
- HIRANO, A., WELCH, R. and LANG, H., 2003, Mapping from ASTER stereo image data: DEM validation and accuracy assessment. *ISPRS Journal of Photogrammetry and Remote Sensing* **57**, pp356-370
- KRAUS, K. and PFEIFER, N., 1998, Determination of terrain models in wooded areas with airborne laser scanner data. *ISPRS Journal of Photogrammetry and Remote Sensing* **53**, pp193-203.
- LIU, X., 2008, Airborne Lidar for DEM generation: some critical issues. *Progress in Physical Geography*. **32**, pp31-49. doi: 10.1177/0309133308089496
- SOUZA, L.C.L., RODRIGUES, D.S. and MENDES, J.F.G., 2003, Sky view factors estimation using a 3D GIS extension. *Proceedings of the 8th International IBPSA Conference*, Eindhoven, Netherlands, August 11-14, 2003.
- STEYN, D.G., 1980, The calculation of view factors from fish-eye lens photographs. *Atmosphere Ocean* **18**, pp254-258
- TELLER, J. and AZAR, S., 2001, Townscope II: Computer system to support solar access decision making. *Solar Energy* **70**, pp187-200.
- UNGER, J., 2007, Connection between urban heat island and sky view factor approximated by a software tool on a 3D urban database. *International Journal of Environmental Pollution* **36**, pp59-80

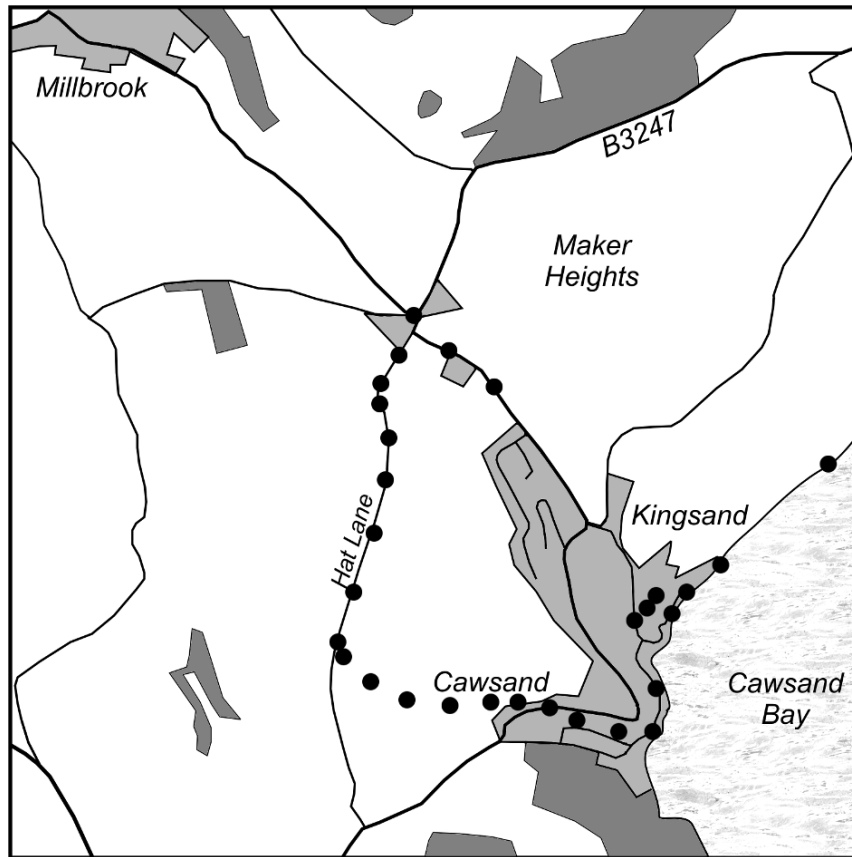


Figure 1. Outline map of the 2 x 2 km study region location in southeast Cornwall (UK). Light grey stipple indicates sea; mid-grey, urban areas and; dark grey, woodland. Dots indicate locations along the transect where photographs for calculation of SVF were taken.

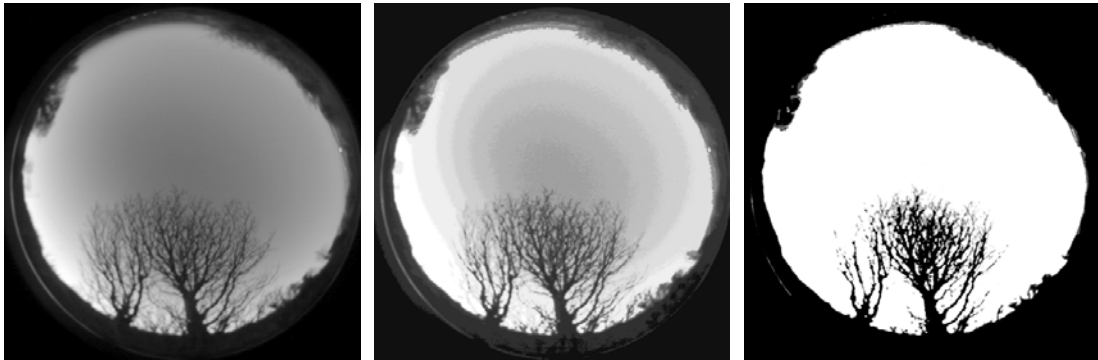


Figure 2. Example of derivation of photographic SVFs: original photograph, 16-class unsupervised classification, and final SVF image with black=non-sky, grey=uncertain, white=sky.



Figure 3. Example of photographic SVFs taken at heights of a) 0 m, b) 1 m and, c) 2m. The associated SVF values are 0.21, 0.34 and 0.50 respectively.

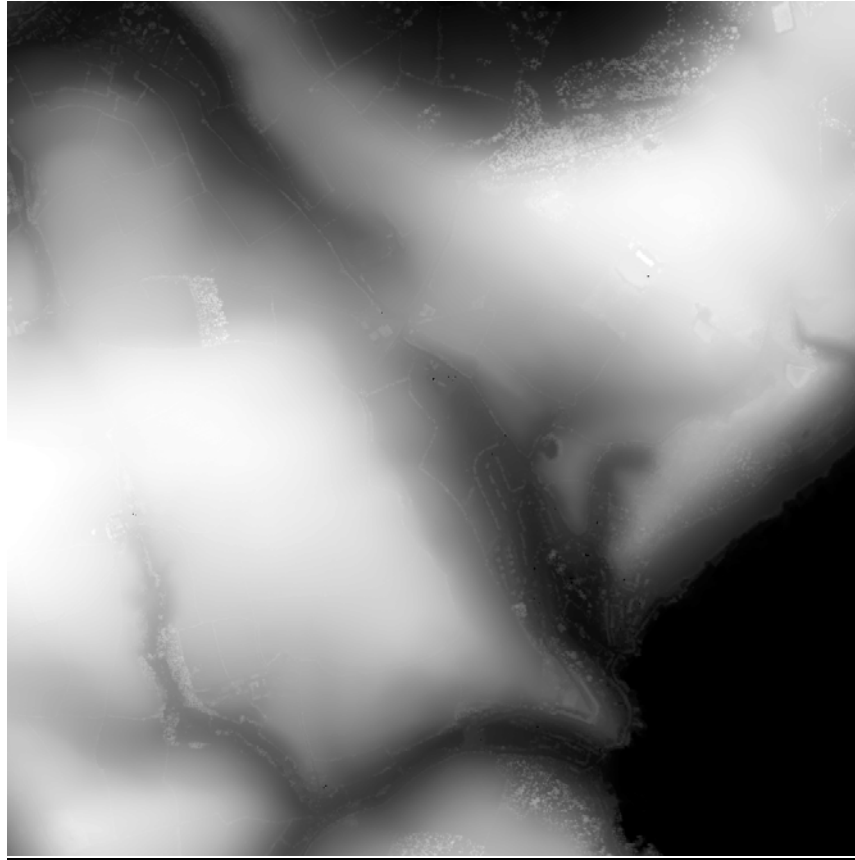


Figure 4. Lidar-derived digital elevation model of the study in SE Cornwall: low elevations are dark, while higher elevations are light. Man-made and woodland features can be seen superimposed on the topological features of the ground surface.

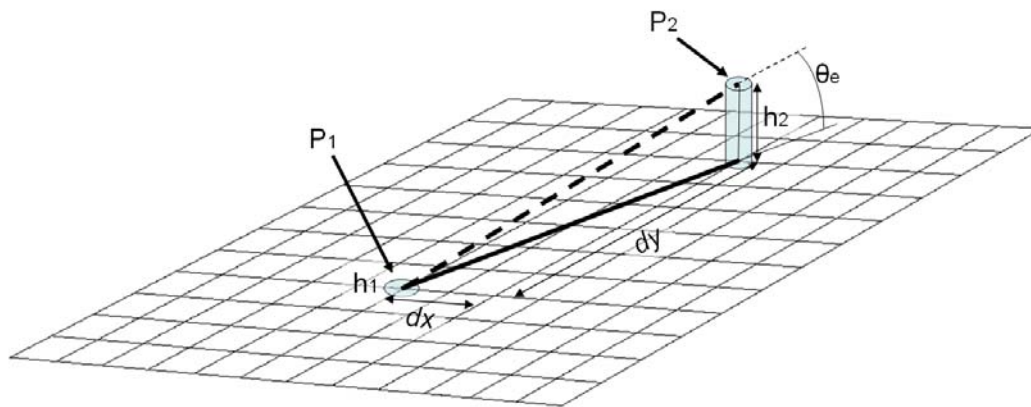


Figure 5. Schematic of the geometry for calculating the sky-view factor: P₁ is the location of the site with a height h₁, P₂ is a distant point with a height of h₂. Using trigonometry the site-distant point elevation angle θ_e can be easily calculated for all azimuth angles and ranges.

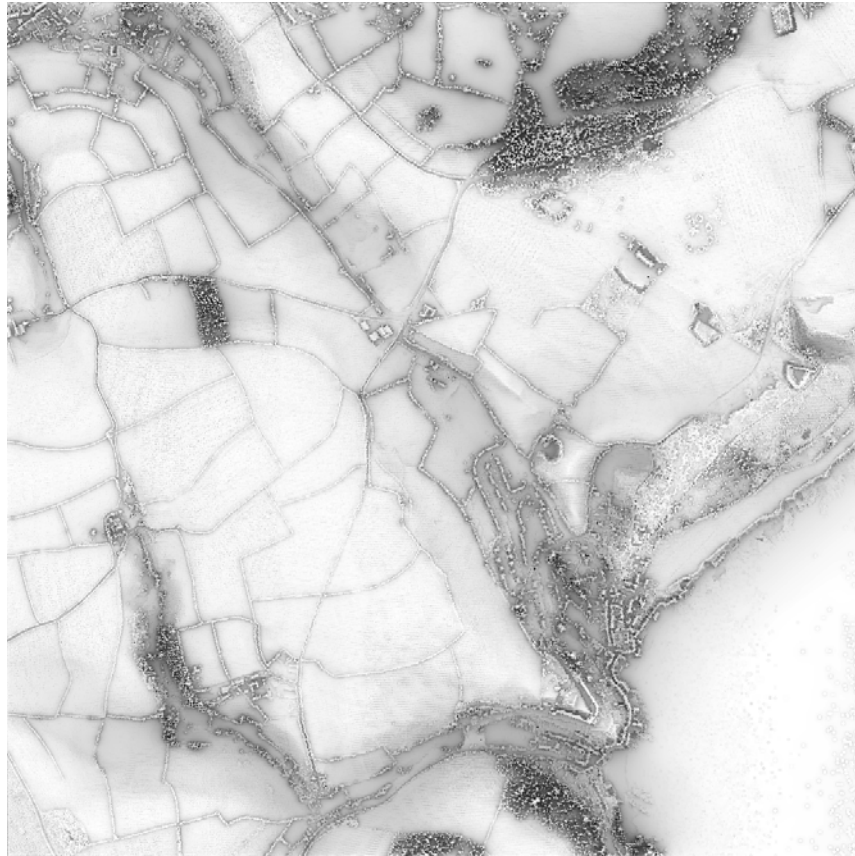


Figure 6. Lidar-derived surface SVF data over the study area. White indicates a SVF of 1 (i.e. clear hemisphere) while black indicates a SVF of zero. The calculation of the SVF highlights the surface texture of the area, in particular the field boundaries, forest/woodland and urban areas/buildings.

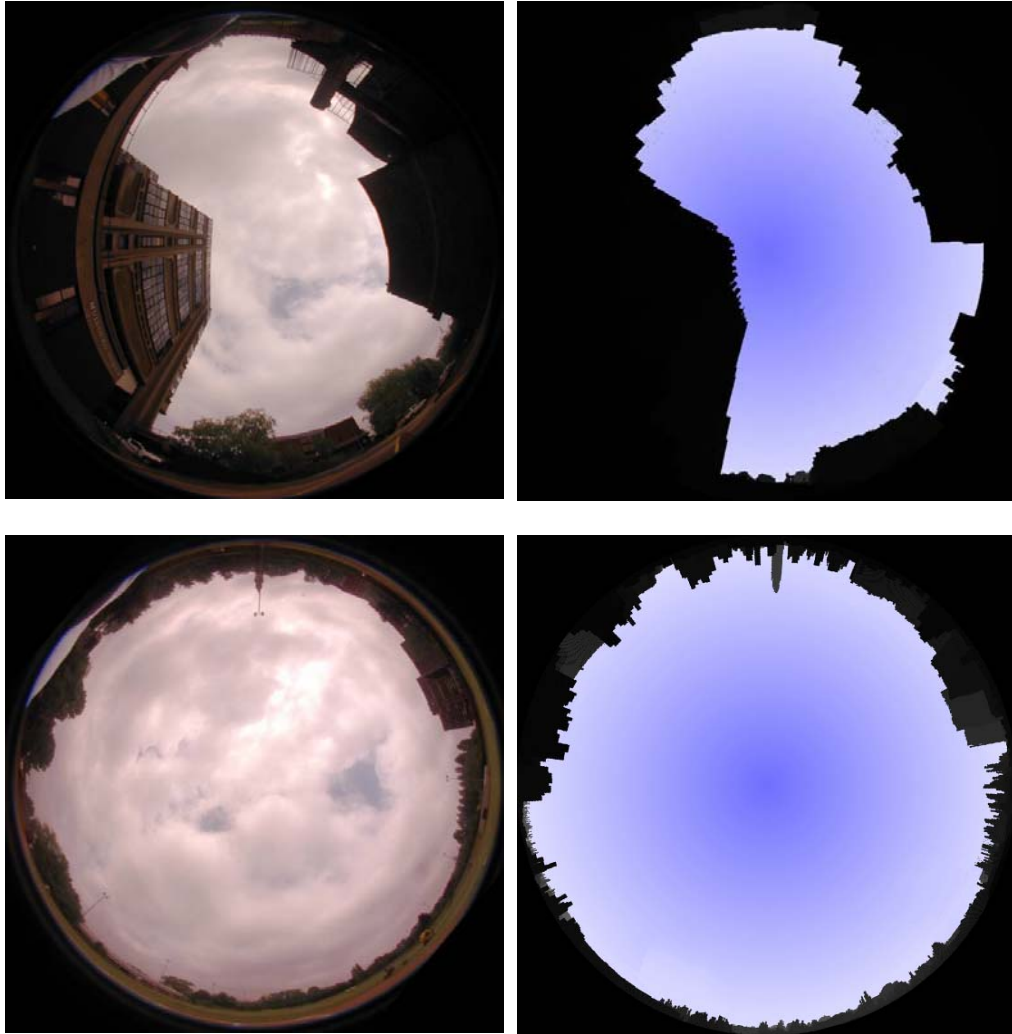


Figure 7. Comparison of conventional fish-eye photographic imagery (left) with Lidar-simulated fish-eye imagery for use in the derivation of SVFs.

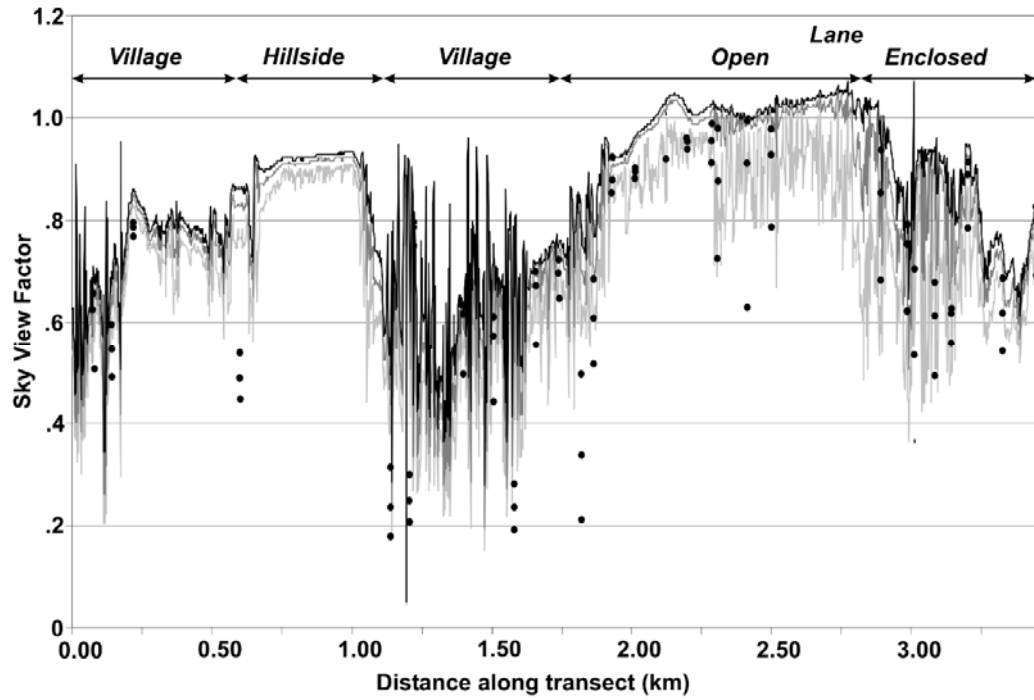


Figure 8. Lidar-derived (lines) and photographic-derived (points) SVF data for the survey transect. The lower line/points are for the surface (0 m), middle line/points for the 1 m measurements and, top line/points for the 2 m measurements.

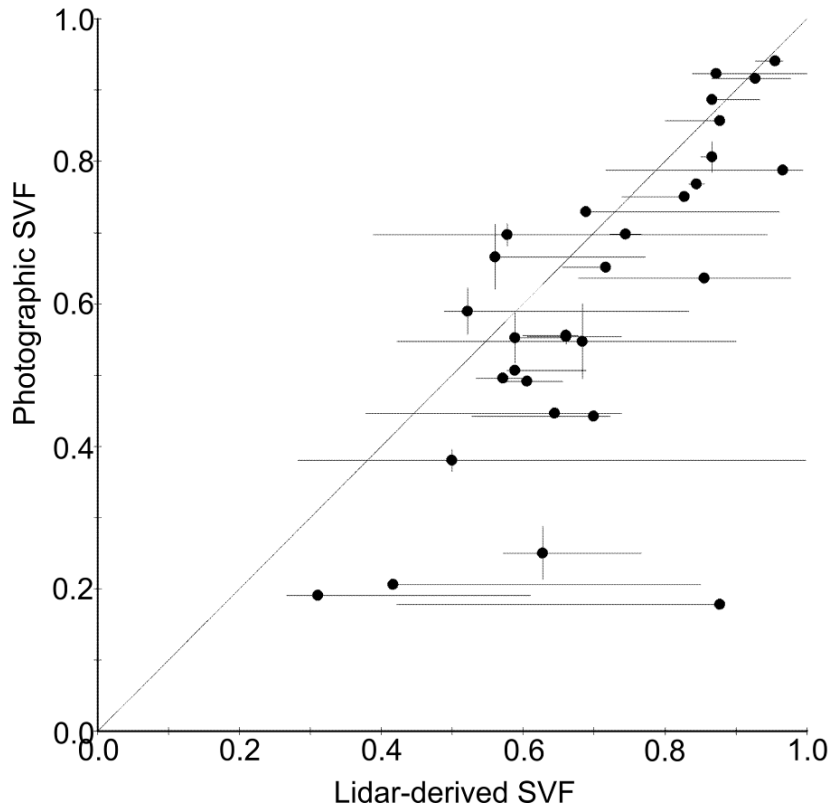


Figure 9(a). Comparison of Lidar-derived SVF and Photographic-derived SVF for surface +0 m. The points represent the samples with the vertical lines showing the uncertainties in the photographic SVF values, while the horizontal lines show the minimum/maximum range in the adjacent Lidar-derived SVF ($R^2 = 0.71$).

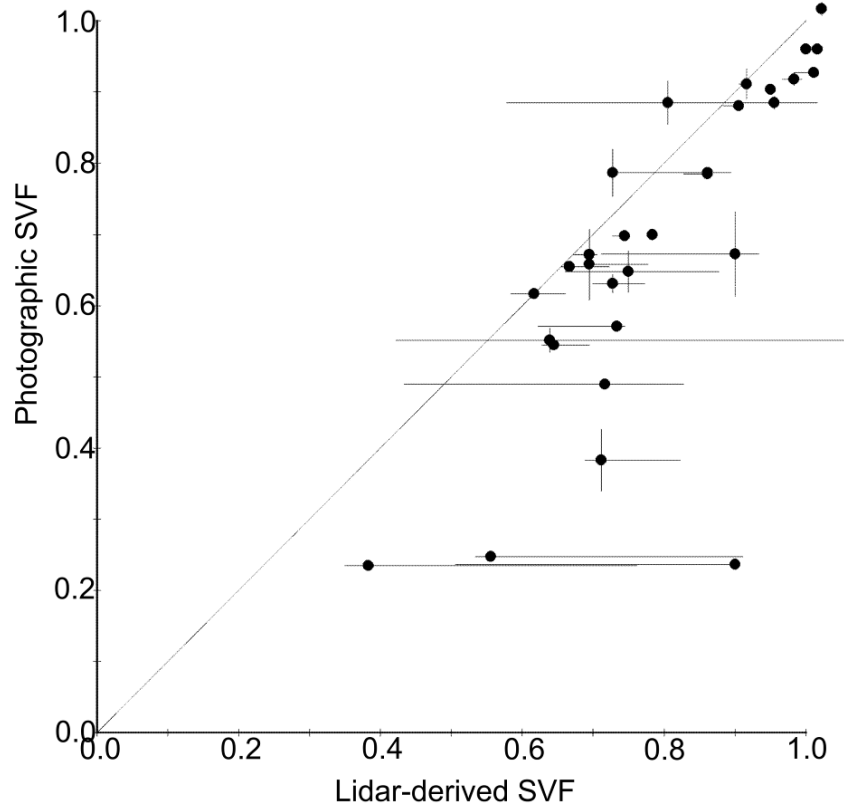


Figure 9(b). As figure 5(a), but surface +1 m. ($R^2 = 0.77$).

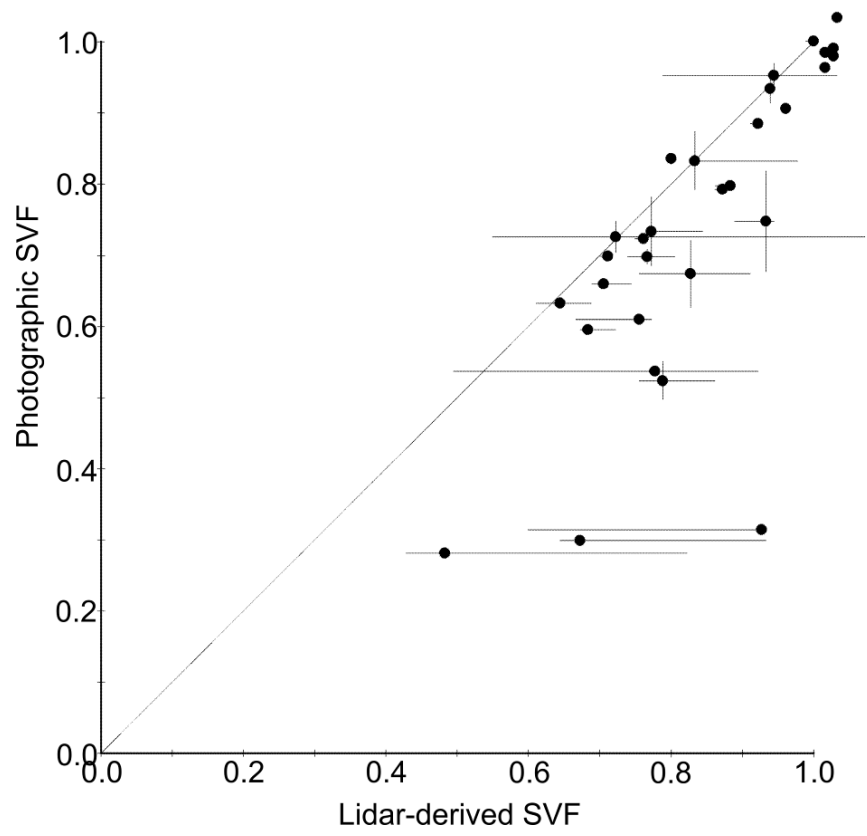


Figure 9(c). As figure 9(a), but surface +2 m. ($R^2 = 0.77$).